Express Polymer Letters Vol.17, No.4 (2023) 406–416
Available online at www.expresspolymlett.com
https://doi.org/10.3144/expresspolymlett.2023.29

Research article

Photoreversible control over ionic conductivity of coumarin-containing poly(ionic liquid)-based solid electrolyte

*Wangjie Xu, Ming Zhang, Yijun Chen, Qinghua Tian, Xianjing Zhou, Li Zhang, Xinping Wang, Wei Zhang**

Key Laboratory of Surface & Interface Science of Polymer Materials of Zhejiang Province, Department of Chemistry, Zhejiang Sci-Tech University, 310018 Hangzhou, China

Received 19 July 2022; accepted in revised form 11 November 2022

Abstract. Poly(ionic liquid)s (PILs) are promising candidates used as solid electrolytes because of their excellent electrochemical properties and improved processability. Introducing light-sensitive groups to PILs appears as an attractive strategy for developing novel smart PIL-based electronic devices. In this work, a new photoresponsive PIL-based solid electrolyte was prepared by blending PILs containing coumarin groups (COU-PILs) with polyvinylidene fluoride hexafluoropropylene. It was found that the ionic conductivity of COU-PIL solid electrolytes (COU-PIL SEs) can be reversibly modulated upon alternative 365 and 254 nm light irradiation. In particular, the COU-PIL SEs exhibit a highly reversible and repeatable manipulation of ionic conductivity with a maximum conductivity modulation of 95%. This reversible control over ionic conductivity is attributed to the photodimerization/photocleavage behavior of the coumarin groups.

Keywords: *smart polymers, poly(ionic liquid)s, ionic conductivity modulation, polymer membrane, mechanical properties*

1. Introduction

Ionic liquids (ILs) exhibit unique properties such as good thermal stability, negligible vapor pressure, high ionic conductivity, and wide electrochemical window. These properties make their corresponding polymers, poly(ionic liquid)s (PILs), promising application in the field of fuel cells, lithium batteries, supercapacitors, and other electrochemical devices [1, 2]. As solid polymer electrolytes in lithium-ion batteries, PILs have been proposed to address the safety issues caused by the leakage of conventional liquid electrolytes [3]. At the same time, light-responsive materials have gained increasing attention as noninvasive, remote, and precise control over their properties can be achieved [4]. These conductive materials with photoresponsive electrochemical properties display potential applications in optical memories and bio-imaging, photodetectors, photocontrolled electronic circuits, and other fields [5–8]. Introducing light-sensitive groups to PILs appears as an attractive strategy for developing novel smart materials. Several studies indicated that the combination of light-responsive molecules and ILs could endow ILs with controllable ionic conductivity. For example, imidazolium-based ILs containing light-sensitive anions of *trans-ortho*-methoxycinnamic acid displayed a ~130% increase in ionic conductivity under 3 h light irradiation in aqueous solutions [9]. Azobenzene-based ILs exhibited reversible tunable ionic conductivity under UV/visible light irradiation with a maximum conductivity modulation of 10.7% [10]. From the view of practical application, PILs are more attractive candidates used as solid electrolytes when compared to ILs because of their

*Corresponding author, e-mail: zhwei@zstu.edu.cn

mechanical stability and improved processability. However, few light-responsive PILs with controllable ionic conductivity have been reported [11, 12]. Recently, Sumitani *et al*. [11] synthesized a light-active PILs containing a ruthenium sandwich cation and a polymeric anion and found that the ionic conductivities of those PILs were reversibly tuned by alternately using light and heat due to a coordination structure transformation. Nie *et al*. [12] incorporated imidazolium containing diarylethenes (DAEs) in a poly(ethylene oxide) backbone and investigated the light-induced conductivity manipulation of the obtained PIL systems. Upon UV/visible light irradiation, the imidazolium containing DAEs switched from a ring-open isomer (having delocalized positive charge) to a ring-closed state (having localized positive charge). In this case, the interaction between mobile anions and DAE-based cations was regulated, and accordingly, the ionic conductivity was reversibly adjusted.

Light-sensitive PILs have shown great potential for the fabrication of smart solid electrolytes. Simple synthesis, high reversibility and desirable conductivity modulation need to be considered for designing and developing light-sensitive PILs. Coumarin and its derivatives are widely used as photoresponsive component because of their high-efficiency reversilibities, excellent biocompatibilities and potentials for dimer formation via visible light [13]. Coumarin derivatives undergo [2+2] cycloaddition when irradiated with a 320~365 nm UV light, while the formed cyclobutane structures can be cleaved when exposed to a ~280 nm light. Incorporating coumarin groups into PILs (COU-PILs) enables the transition between crosslinking and decrosslinking among their chains upon irradiation with different light sources, which will cause the change in ion transport behavior through a polymer matrix.

In this work, we designed a photosensitive PIL-based solid electrolyte to achieve reversible conductivity modulation. The photosensitive COU-PILs were prepared by a simple radical polymerization of quaternary ammonium-type IL monomer containing coumarin groups ($[DMAEMA\text{-}COU]^+[Br]^-$), and subsequently an anion exchange reaction (Figure 1). Since these COU-PILs themselves could hardly form a robust film, they were generally blended with polyvinylidene fluoride hexafluoropropylene (PVDF-HFP) to improve mechanical strength of the blend film [14]. The reversible change in ionic conductivity of the obtained coumarin-containing PIL solid electrolytes (COU-PIL SE) film was investigated in detail. It was shown that the ionic conductivity of COU-PIL SE films was manipulated with high-efficiency reversibility when irradiating these films with alternative 365 and 254 nm light. The results indicate a novel insight into the fabrication of smart photocontrollable devices and wearable photodetectors.

2. Experimental

2.1. Materials

7-Hydroxycoumarin (99%) was purchased from Meryer Chemical Technology Co., Ltd. (Shanghai, China) 2-(Dimethylamino)ethyl methacrylate (DMAEMA) (99%), azodiisobutyronitrile (AIBN) (99%), and butylated hydroxytoluene (BHT) were obtained from Macklin Inc. (Shanghai, China). 1,3-Dibromopropane (99%), lithium bis(trifluoromethanesulfonimide) (LiTFSI) (99%), potassium carbonate (K_2CO_3) (99%), and magnesium sulfate ($MgSO_4$) (99%) were supplied by Aladdin Chemistry Co. Ltd. (Shanghai, China). Polyvinylidene difluoroethylene hexafluoropropylene (PVDF-HFP) (M_w ~455 000 g/mol) was purchased from Sigma-Aldrich (St. Louis, USA). The monomer of DMAEMA was passed through a column of the neutral aluminum oxide in order to remove the added inhibitors. Solvents, including dichloromethane (DCM), acetone, methanol, dimethyl formamide (DMF), and dimethyl sulfoxide (DMSO), were of analytical grade and were used without further purification.

2.2. Characterization

The chemical structure of products was identified by ^1H and ^{13}C nuclear magnetic resonance spectrometry (NMR) using a BruckerAvance II DMX spectrometer (Bruker, Germany) operating at 400 MHz. Energy-dispersive X-ray spectroscopy (EDX) was used to determine the element content of COU-PILs with field-emission scanning electron microscopy (Hitachi SU8010, Japan). Fourier transform infrared (FTIR) spectra were collected at room temperature using a Nicolet Avatar 370 spectrometer (Thermo Nicolet Co., USA) in the range of 4000–400 cm^{-1}. The glass transition temperature (T_g) was obtained with a differential scanning calorimeter (DSC, TA Q2000, TA Instruments, USA) at temperatures ranging from –50 to 180 °C. Samples (5–10 mg) were encapsulated in standard aluminum pans, heated/cooled at a rate of 10 °C·min^{-1} under N_2 protection, and the

data during the first cooling were analyzed. Dynamic mechanical analysis (DMA) was conducted with a dynamic mechanical analyzer (Q800, TA Instruments, America) at a fixed frequency of 1 Hz over a temperature range of 20–150 °C with a heating rate of 5 °C·min^{-1}. The mechanical properties of samples were measured on a QL-5 instrument (OBT Testing Equipment, Jinan, China) at room temperature with a stretch speed of 2 mm/min.

The reversible photoresponse of the coumarin-containing PIL system was assessed using UV-Vis absorbance spectroscopy on a UV-Vis spectrophotometer (UV-2600, Shimadzu, Japan) at the scan speed of 200 nm·min^{-1}. An initial spectrum in the unexposed state was collected, and the sample was then irradiated with 365 nm UV light for different periods of time. The UV-Vis spectra were recorded until the equilibrium state was reached, followed by exposure to 254 nm UV light for different periods of time.

The ionic conductivity (σ) of the COU-PIL SE film was tested by impedance spectroscopy measurements with a CHI660D electrochemical workstation (Shanghai Chenhua Instrument, Shanghai, China). The films were sandwiched between two stainless steel (SS) plate electrodes. The spectra were recorded in the frequency range of 0.01 Hz–1 MHz with an alternating current (AC) amplitude of 5 mV. The σ values of the films were calculated according to Equation (1):

$$\sigma = \frac{L}{RS} \tag{1}$$

where R and L are the bulk resistance and film thickness, respectively, and S is the area of the steel electrode. The power of 365 and 254 nm light was 3 and 15 W, respectively.

2.3. Synthesis of 7-(3-bromopropyloxy) coumarin

The synthetic route of 7-(3-bromopropyloxy) coumarin was shown in Figure 1, and the exact experimental process was conducted according to previous methods [15]. 1,3-Dibromopropane (10 g, 50 mmol) and K_2CO_3 (10 g, 72 mmol) was dissolved in 50 ml acetone in a 200 ml round-bottom flask and started to reflux at 50 °C. Next, 7-hydroxycoumarin (810 mg, 5 mmol) was added dropwise to the obtained mixture within 30 min and refluxed for an additional 2 h. After the reaction was complete, the acetone was evaporated, and the mixture was partitioned between 100 ml DCM and water. The DCM layer was collected, and the water was extracted twice with 100 ml DCM; then, the combined DCM layers were dried with $MgSO_4$. After drying, the product 7-(3-bromopropyloxy) coumarin was obtained (orange powder, yield: 82%). ^{1}H NMR (400 MHz, $CDCl_3$) δ: 7.64 (d, J = 9.5 Hz, 1H), 7.38 (d, J = 8.3 Hz, 1H), 6.88–6.81 (m, 2H), 6.26 (d, J = 9.5 Hz, 1H), 4.18 (t, J = 5.8 Hz, 2H), 3.61 (t, J = 6.4 Hz, 2H), 2.36 (p, J = 6.1 Hz, 2H). ^{13}C NMR (101 MHz, $CDCl_3$) δ: 161.9, 161.1, 155.9, 143.4, 128.9, 113.3, 112.9, 112.8, 101.6, 101.5, 66.0, 64.8, 32.0, 29.6.

2.4. Synthesis of quaternary ammonium-type IL monomer ([DMAEMA-COU]$^+$[Br]$^-$)

7-(3-Bromopropyloxy) coumarin (1.558 g, 5.5 mmol), DMAEMA (786 mg, 5 mmol), polymerization inhibitor BHT (22 mg, 0.1 mmol), and 15 ml acetone were added into a 100 ml round bottom flask and were mixed by vigorously stirring. The reaction was carried out at 50 °C for 24 h under a nitrogen atmosphere. The resultant product was thoroughly washed

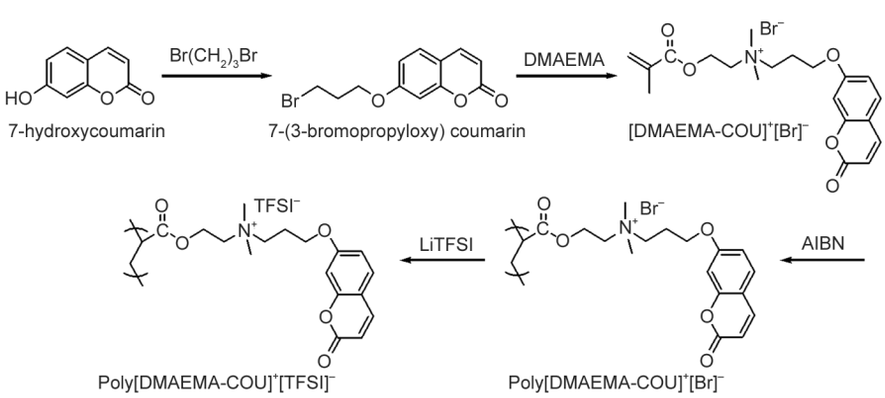

Figure 1. Schematic for the synthesis of photosensitive quaternary ammonium-type poly(ionic liquid)s (PILs) containing coumarin groups, poly([DMAEMA-COU]$^+$[TFSI]$^-$).

with acetone at least 3 times and dried under vacuum at 40 °C for 24 h. The obtained [DMAEMA-COU]$^+$[Br]$^-$ is a pale yellow powder with a yield of 69%. ^{1}H NMR (400 MHz, D_2O) δ: 7.79 (dd, J = 9.5, 2.0 Hz, 1H), 7.41 (dd, J = 8.8, 2.0 Hz, 1H), 6.83 (dt, J = 8.7, 2.3 Hz, 1H), 6.73 (d, J = 2.4 Hz, 1H), 6.17 (dd, J = 9.5, 2.0 Hz, 1H), 6.06 (s, 1H), 5.63 (d, J = 1.8 Hz, 1H), 4.65–4.47 (m, 2H), 4.23–4.02 (m, 2H), 3.79 (dd, J = 6.3, 3.5 Hz, 2H), 3.71–3.47 (m, 2H), 3.19 (d, J = 2.0 Hz, 6H), 2.37–2.20 (m, 2H), 1.82 (d, J = 1.9 Hz, 3H). ^{13}C NMR (101 MHz, DMSO-d_6) δ: 166.4, 161.8, 160.7, 155.8, 144.8, 135.9, 130.1, 127.2, 113.2, 113.2, 113.1, 101.8, 66.1, 62.5, 61.9, 58.6, 51.2, 22.6, 18.4.

2.5. Synthesis of poly([DMAEMA-COU]$^+$[Br]$^-$)

Poly([DMAEMA-COU]$^+$[Br]$^-$) was prepared via free radical polymerization (Figure 1). IL monomer [DMAEMA-COU]$^+$[Br]$^-$ (2.203 g, 5 mmol), initiator AIBN (44.1 mg, 0.27 mmol), and methanol (20 ml) were added into a three-necked flask. After the mixtures were completely degassed, the reaction was conducted at 65 °C for 24 h under a nitrogen atmosphere. Since poly([DMAEMA-COU]$^+$[Br]$^-$) was insoluble in methanol, the precipitation would appear upon polymerization. After polymerization, the obtained products were washed with methanol 3 times and then dried under vacuum at 40 °C for 24 h. Poly([DMAEMA-COU]$^+$[Br]$^-$) (yield: 80%) is yellow powder. ^{1}H NMR (400 MHz, DMSO-d_6) δ: 7.97 (s, 1H), 7.60 (s, 1H), 6.90 (s, 2H), 6.25 (s, 1H), 4.85 (s, 2H), 4.18 (s, 2H), 3.42 (s, 1H), 3.29 (s, 1H), 2.28 (s, 2H), 1.00 (s, 3H).

2.6. Synthesis of poly([DMAEMA-COU]$^+$[TFSI]$^-$)

Poly([DMAEMA-COU]$^+$[TFSI]$^-$) was prepared via an anion exchange reaction. LiTFSI (3.445 g) and poly([DMAEMA-COU]$^+$[Br]$^-$) (4.406 g) were dissolved in 50 ml DMSO, and the solution was stirred at room temperature for 12 h, followed by extraction with excessive deionized water. After drying at 80 °C for 48 h under vacuum, the poly([DMAEMA-COU]$^+$[TFSI]$^-$) was obtained (yellow powder, yield: 89%). As shown in Figure 2, energy-dispersive X-ray spectroscopy (EDX) revealed that there was no Br$^-$ remaining in poly([DMAEMA-COU]$^+$[TFSI]$^-$), indicating a complete anion exchange reaction.

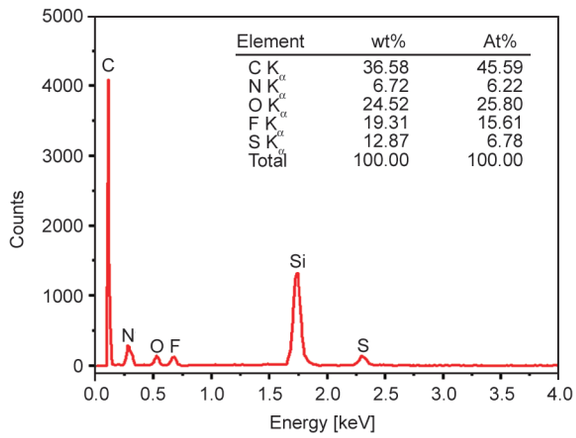

Figure 2. EDX spectra of poly([DMAEMA-COU]$^+$[TFSI]$^-$).

2.7. Preparation of coumarin-containing PIL solid electrolyte films

In order to prepare photosensitive polymers, coumarin groups were introduced to quaternary ammonium-type poly(ionic liquid)s (PILs). The obtained PILs were denoted as COU-PILs. Since these COU-PILs themselves could hardly form a robust film, they are normally blended with PVDF-HFP, widely used solid electrolyte materials for improving mechanical strength [16, 17]. In this work, the COU-PIL SE films were prepared by blending COU-PILs, PVDF-HFP, and LiTFSI, as shown in Figure 3. The COU-PILs, namely, poly([DMAEMA-COU]$^+$[TFSI]$^-$) and PVDF-HFP, were dissolved in DMSO, and the

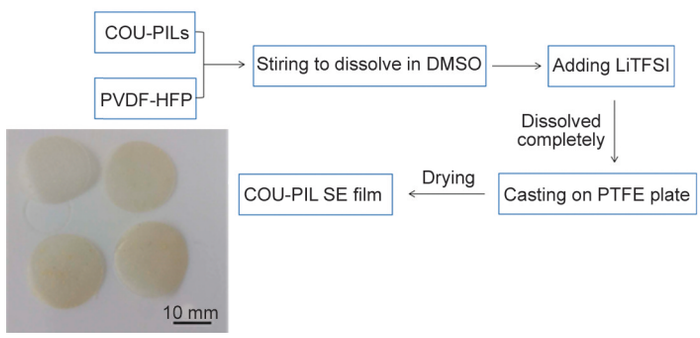

Figure 3. Preparation of the COU-PIL SE film.

blending ratio by weight of COU-PILs to PVDF-HFP was varied from 10/90 to 50/50. Then, LiTFSI (20% of the total weight) was added to the mixture. After complete dissolving, the resulting solution was cast onto a polytetrafluoroethylene (PTFE) plate with a casting knife. The obtained film was further dried in a vacuum oven at 80 °C for 48 h. The thickness of the COU-PIL SE films is 200±20 μm.

3. Result and discussion

3.1. Effect of COU-PILs/PVDF-HFP blending ratio on ionic conductivity and mechanical properties

A series of COU-PIL SE films were prepared by varying the COU-PILs/PVDF-HFP blending ratio while keeping the LiTFSI content unchangeable in order to explore the effect of COU-PILs content on film properties. The effect of COU-PILs content on the ionic conductivity of COU-PIL SE films is presented in Figure 4a. As expected, the ionic conductivity of the COU-PIL SE film increased with increasing COU-PILs content. As shown in Figure 4b, on the other hand, the tensile strength of the COU-PILs SE film decreased while the tensile strain increased as increasing COU-PILs content. This seemed reasonable because COU-PILs themselves have low mechanical strength and even could hardly form a robust film. For example, the film with COU-PILs/PVDF-HFP blending ratio of 50:50, displayed the highest ionic conductivity but lower mechanical properties (tensile strength: 1.86 MPa, Young's modulus: 15.38 MPa) among those SE films. However, this mechanical property was still better than the conventional PEO electrolyte films and other solid electrolyte films reported in the literature [18, 19]. By considering ionic conductivity and mechanical property comprehensively, the COU-PIL SE film with the COU-PILs/PVDF-HFP blending ratio of 50:50 was used for the next investigation.

3.2. Structural photo responsiveness of COU-PIL SE film

The structures of COU-PIL SEs are tuned by taking advantage of the reversible photoresponse of coumarin groups of PILs. Upon 365 nm irradiation, as shown in Figure 5, dimerization occurred between PIL chains to form a cross-linked structure, and the movement of the polymer segments would be hindered. After 254 nm UV irradiation, however, the dimer dissociated to return to the original structure.

The dimerization of COU-PILs can be confirmed by FTIR spectroscopy. Upon 365 nm light irradiation,

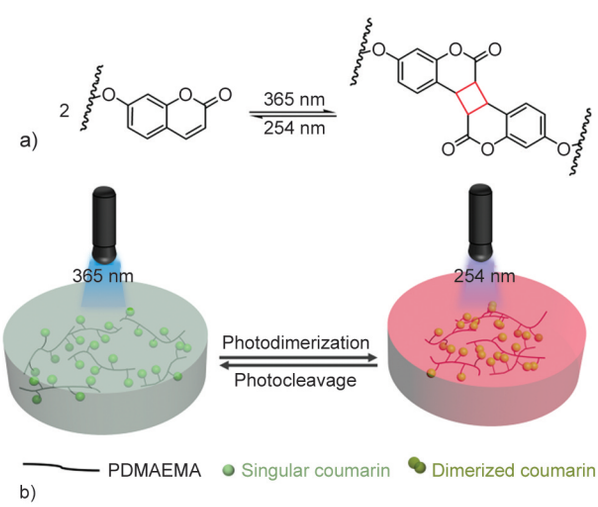

Figure 5. a) Reversible dimerization and cleavage of coumarin groups upon exposure to 365/254 nm light. b) Schematic diagram of crosslinking network formation and dissociation.

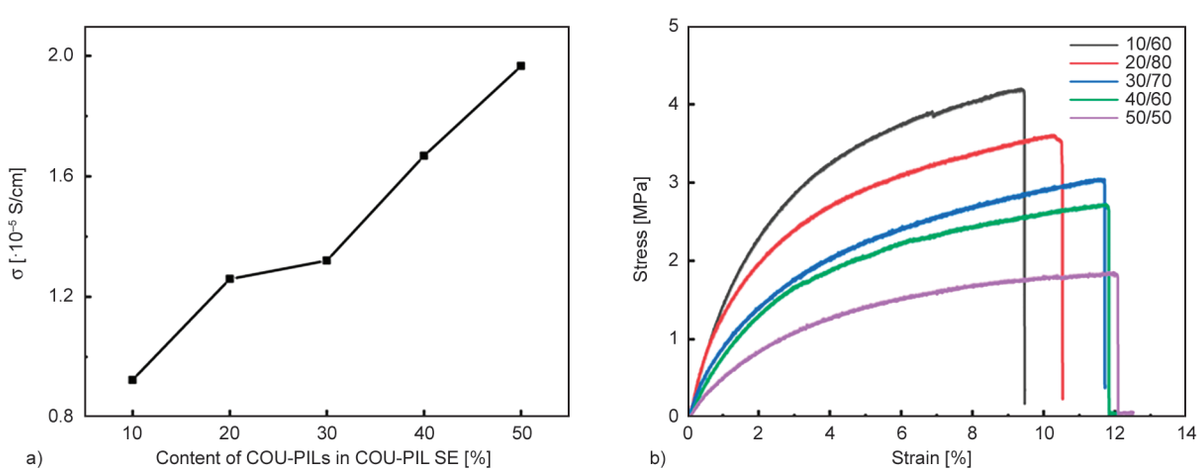

Figure 4. a) Ionic conductivity and b) stress-strain curves of COU-PIL SE films with different COU-PILs/PVDF-HFP blending ratios.

as shown in Figure 6, the intensity of the peak at 1616 cm^{-1} (ring C=C stretching vibration) decreased almost double when compared to the initial samples. In addition, a small shoulder peak appeared at 1765 cm^{-1}, which was attributed to the carbonyl stretching of the H–H dimer [20]. Upon exposure to 254 nm light, COU-PILs SE films displayed almost the same FTIR spectra as the initial samples, namely, those before 365 nm light irradiation. Those changes in FTIR spectra demonstrate the occurrence of photodimerization and photocleavage of coumarin units in the blending matrix.

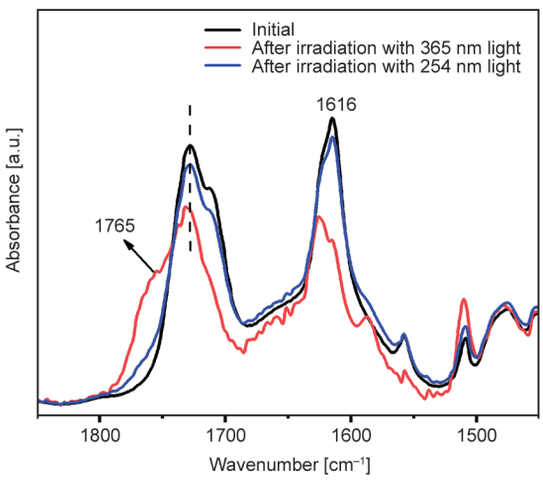

Figure 6. FTIR spectra of COU-PIL SE films after 365/254 nm light irradiation and before 365 nm light irradiation.

Further detection of the photodimerization and photocleavage of coumarins units was conducted by using UV-Vis absorption spectroscopy. As shown in Figure 7a, the maximum absorption peak at 324 nm was attributed to the coumarin double bond. The intensity of this peak gradually decreased when irradiated with a 365 nm light, suggesting the dimerization of coumarin groups [21]. Followed by the exposure to 254 nm light, the absorption intensity at 324 nm increased gradually (Figure 7b), implying that the formed coumarin dimers were cleaved. The change in the maximum absorption peak clearly indicated that the structural transition of COU-PILs

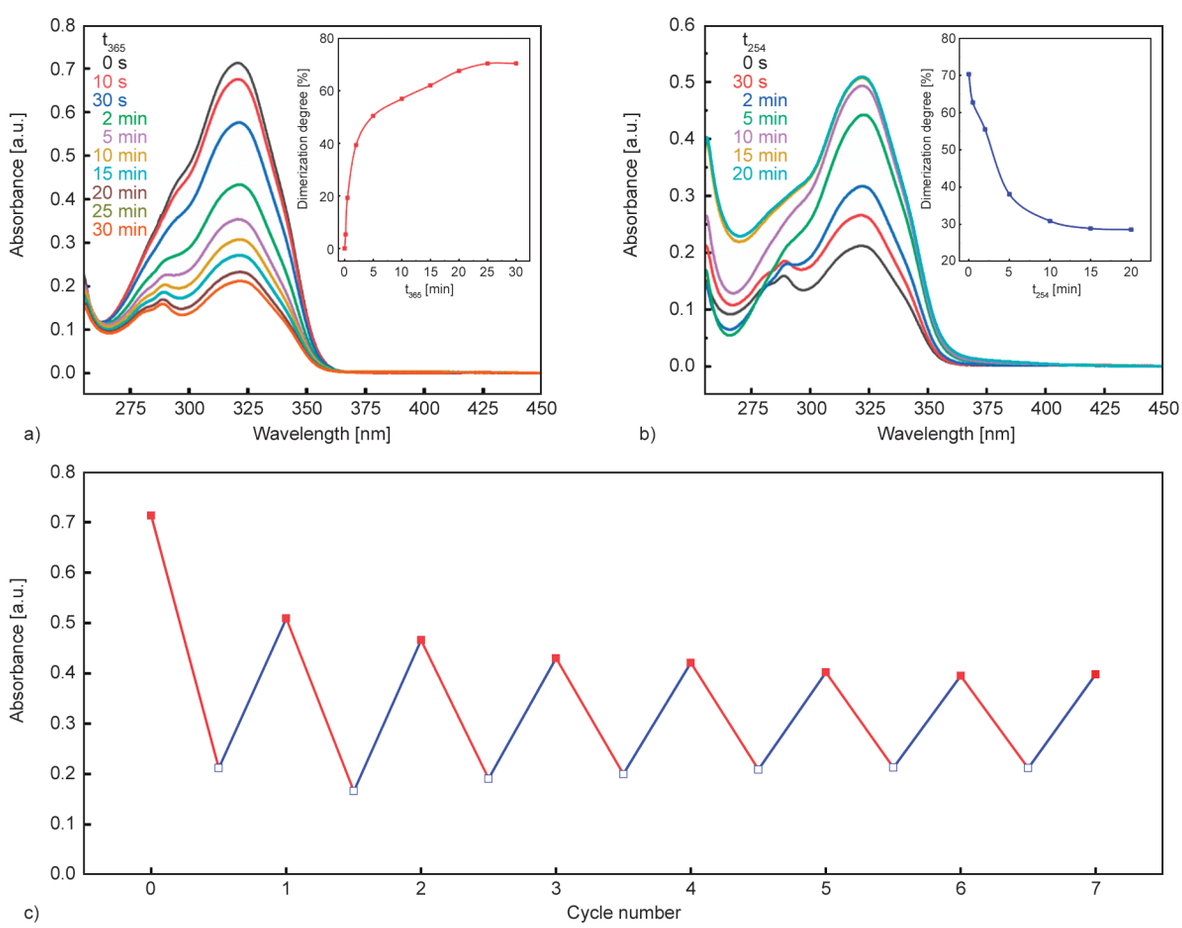

Figure 7. UV-Vis absorption spectra of COU-PIL SE film upon light irradiation at the wavelength of a) 365 nm, b) 254 nm. c) Absorption at 324 nm for COU-PIL SE film during 7 cycles. Insets in a) and b) show the variations of dimerization degree with light irradiation time.

was reversibly tailored under light irradiation, which makes it possible to control the ionic conductivity of the COU-PIL SE film.

The light-induced structural change can also be evaluated by the dimerization degree, D, using Equation (2):

$$D = \frac{A_0 - A_t}{A_0} \cdot 100\% \quad (2)$$

where A_0 is the absorbance at 324 nm of the pristine film and A_t is the absorbance of the film at irradiation time t (t_{365} and t_{254} mean 365 and 254 nm light irradiation, respectively) [22]. It can be seen from the insets of Figure 7 that D gradually increased with t_{365} and finally attained the maximum of 70% within 25 min, while it decreased with t_{254} and reached an equilibrium value of 28% within 20 min.

It was worth noting that D did not attain zero even for prolonging light irradiation at 254 nm because photocleavage and photodimerization of coumarin groups occurred simultaneously upon 254 nm light exposure [22–25]. For convenient comparison, one photodimerization followed by one photocleavage is defined as one cycle. As mentioned above, the absorption at 324 nm could attain equilibrium when exposed to 365 and 254 nm for 25 and 20 min, respectively. Here we employed the equilibrium absorption at 324 nm to evaluate the light-induced reversibility. Figure 7c presents the change in equilibrium absorption at 324 nm during at least 7 cycles. The maximum absorption decreased from 0.7 in the first cycle to 0.5 in the second cycle and finally 0.4 after 7 cycles, implying that some of the formed coumarin dimers were not cleaved. This was possibly attributed to the asymmetric fission of coumarin dimer during photocleavage under 254 nm light that resulted in irreversible crosslinking [22, 26]. This decay in photoreversibility was unfavorable for the tunable performance modulation. Fortunately, it could be addressed by adding photosensitizer or increasing the power intensity of the light [24, 27].

3.3. Photoresponsiveness of ionic conductivity of COU-PIL SE film

Noticeably, the ionic conductivity varies with irradiation time and finally attains an equilibrium value. For the COU-PIL SE film containing 50% COU-PILs, the time for ionic conductivity to approach equilibrium are 25 and 20 min for 365 and 254 nm irradiation, respectively. The kinetics of ionic conductivity are not listed here, and only the equilibrium values are given in Figure 8 in order to show the repeatable change of ionic conductivity clearly. As presented in Figure 8a, in the first cycle, the ionic conductivity decreased from $1.96 \cdot 10^{-5}$ to $2.32 \cdot 10^{-6}$ S·cm^{-1} at 25 °C after 365 nm light irradiation within 25 minutes, suggesting that light irradiation decreased the ionic conductivity by more than an order of magnitude. When the 254 nm light was employed, the ionic conductivity increased significantly and attained 90% of its original value, which may be due to an incomplete decrosslinking. In fact, the photodimerization and photocleavage of coumarin groups themselves are typically time-dependent, and even 60 min are required for photodimerization to approach equilibrium [22, 25]. This time dependence may be due to the confined light-induced structural evolution caused by the lower mobility of polymer

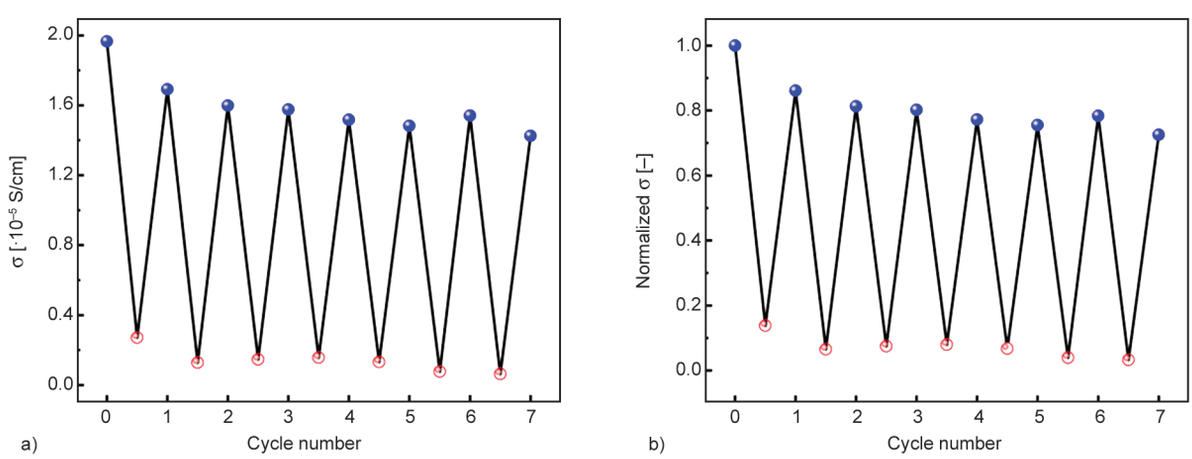

Figure 8. Reversible change in a) the ionic conductivity and b) normalized ionic conductivity of COU-PIL SE film exposed to alternative 365 nm light for 25 min (red hollow symbol) and 254 nm light for 20 min (solid blue symbol). The ratio of COU-PILs and PVDF-HFP in the SE film is 50/50.

chains. In the subsequent cycle, however, the ionic conductivity could be switched back to the starting value, namely about $1.6 \cdot 10^{-5}$ S·cm^{-1}, upon 254 nm light irradiation. The change in ionic conductivity with light irradiation can be repeated at least 7 cycles, implying an excellent reversible modulation. The desirable repeatability of conductivity modulation can also be clearly seen in Figure 8b. The normalized σ fluctuated in the range of 0.05~0.9 over 7 cycles, and the maximum conductivity modulation was as high as 95%. Such a high modulation indicates the efficient control of ionic conductivity, which is favorable for various applications. In addition, these results agreed well with those of dimerization as detected by UV-Vis absorption spectroscopy (Figure 7), implying that the photodimerization and photocleavage of coumarin units resulted in the reversible conductivity modulation. It should be pointed out that when the COU-PIL SE films were irradiated by 254 nm light in every cycle, their ionic conductivities can recover to about $(1.5\sim1.7) \cdot 10^{-5}$ S·cm^{-1} at room temperature (Figure 8a), which is higher than the minimum value of 10^{-5} S·cm^{-1} (at 25 °C) required for acceptable battery performance [28, 29]. This means that the COU-PIL SE film can be reversibly switched between conductive and non-conductive states under alternating illumination of 365 and 254 nm light.

When the ratio of COU-PILs and PVDF-HFP in the blending SE film was varied from 10/90 to 40/60, the reversible behavior of conductivity was still observed (Figure 9). In order to better show the effect of COU-PILs component on reversible conductivity modulation, the magnitude of the modulation of the ionic conductivity (Δσ) was calculated using Equation (3):

$$\Delta\sigma = \frac{\sigma_0 - \sigma_t}{\sigma_0} \tag{3}$$

where σ_0 is the conductivity of the unexposed state and σ_t is the conductivity after 365 nm UV irradiation [10]. It can be observed from Figure 10 that the

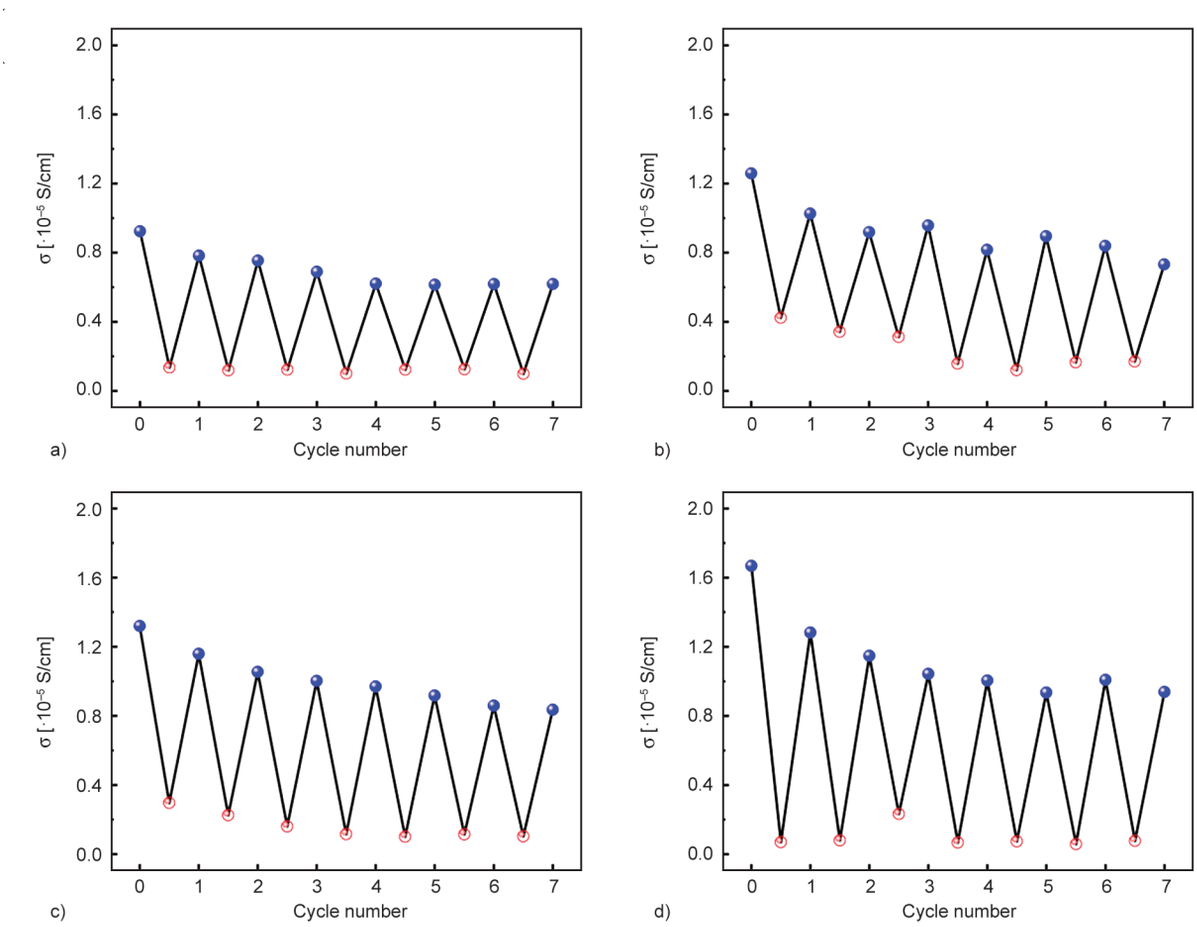

Figure 9. Reversible change in the ionic conductivity of the COU-PIL SE films exposed to alternative 365 nm light for 25 min (solid blue symbol) and 254 nm light for 20 min (red hollow symbol). The weight ratio of COU-PILs and PVDF-HFP is a) 10:90, b) 20:80, c) 30:70, d) 40:60.

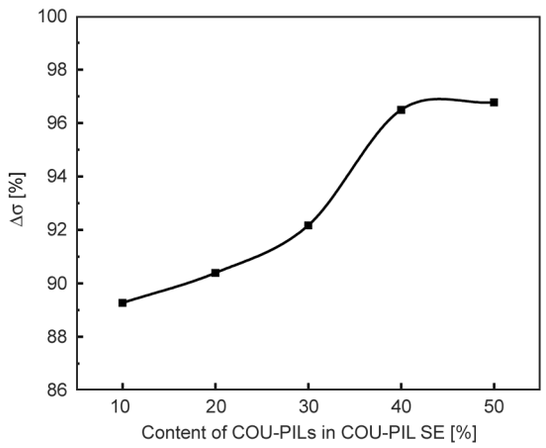

Figure 10. Conductivity modulation of the COU-PIL SE films as a function of the weight ratio of COU-PILs and PVDF-HFP under 7 cycles of illumination.

tunable magnitude of ionic conductivity was enhanced with increasing the COU-PILs content in the blending film, supporting that the COU-PILs components had played an important role in conductivity modulation.

3.4. Reversible manipulation mechanism

It is well documented that Li ions are transported in a polymer matrix via hopping from one coordinating site to another, attaching to polymer backbone or side chains [30, 31]. The segmental motion of polymer chains facilitates the ions' transport, thus improving the ionic conductivity. Conversely, fabricating crosslinking network in a polymer matrix can decrease the ionic conductivity of the polymer electrolyte by restraining the mobility of polymer chains [32]. Incorporating coumarin groups into the polymer matrix can achieve the reversible formation of crosslinking structures [14, 25], which provides a feasible strategy for reversible photocontrol over ionic conductivity. Herein, the degree of crosslinking of COU-PIL SE film upon successive 365 and 254 nm light irradiation was evaluated by dynamic mechanical analysis (DMA) to understand better the reversible behavior of ionic conductivity in our system. The modulus values shown in Figure 11 are utilized to calculate the crosslinking density, namely, the number of moles of network chains per cubic meter (ν_e), using Equation (4) [33]:

$$\nu_e = \frac{E'}{3RT} \tag{4}$$

where E' is the storage modulus, R is the universal gas constant and T is the temperature ($T > T_g$). As listed in the inset of Figure 11a, there was a significant increase in ν_e upon 365 nm light irradiation. Once irradiated by 254 nm light, however, the ν_e value decreased dramatically despite the incomplete recovery. Similar behavior was also observed in the first cycle modulation, as shown in Figure 6 and Figure 7. The segmental motion of polymer chains can also be reflected by the change of T_g. In order to clearly show the change in T_g, the DSC curves in the temperature range of –15 to 75 °C are provided. As shown in Figure 11b, the initial COU-PIL SE film without illumination displayed a lower T_g of –0.5 °C, which probably resulted from the plasticization of LiTFSI [14]. The T_g increased to 41.1 °C upon 365 nm light irradiation while decreased to 14.2 °C upon 254 nm light irradiation. The decrease of T_g meant increased free volume, which provided more

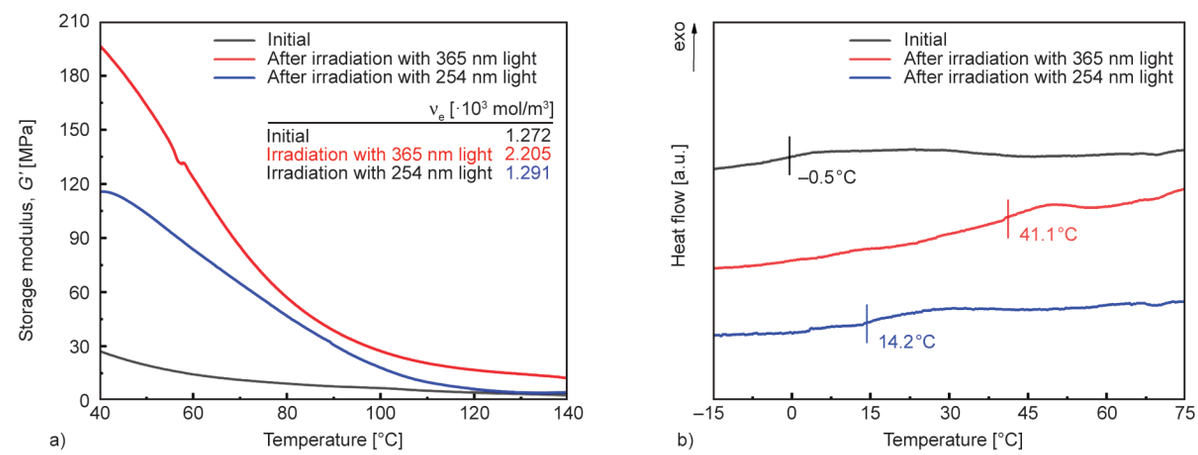

Figure 11. DMA (a) and DSC (b) curves of COU-PIL SE film upon light irradiating at different wavelengths. Inset in a) gives the crosslinking density before and after light irradiation.

free space for Li ions to migrate in the polymer matrix. These results indicated that the photodimerization and photocleavage of coumarin components led to the change of polymer segmental motion, producing reversible conductivity modulation.

4. Conclusions

We have developed a coumarin-containing PIL-based solid electrolyte whose ionic conductivity can be reversibly tailored by photoirradiation. Upon 365 nm light irradiation, the ionic conductivity decreased, whereas it increased upon the subsequent light irradiation at 254 nm. This process can be repeated at least 7 times, within which the maximum conductivity modulation was as high as 95%. The controllable conductivity was attributed to the reversible formation of crosslinking structures caused by photodimerization and photocleavage of coumarin components. This strategy for fabricating a light-responsive PIL-based polymer electrolyte provides a novel idea for the development of functional materials such as smart photo-controllable devices and wearable photodetectors.

Acknowledgements

The authors acknowledge the financial support from the Natural Science Foundation of Zhejiang Province (LY13B040004) and the National Natural Science Foundation of China (21978274 and 21704092).

References

[1] Zhang S. Y., Zhuang Q., Zhang M., Wang H., Gao Z., Sun J-K., Yuan J.: Poly(ionic liquid) composites. Chemical Society Reviews, **49**, 1726–1755 (2020). https://doi.org/10.1039/C8CS00938D

[2] Zhang D-Z., Ren Y-Y., Hu Y., Li L., Yan F.: Ionic liquid/poly(ionic liquid)-based semi-solid state electrolytes for lithium-ion batteries. Chinese Journal of Polymer Science, **38**, 506–513 (2020). https://doi.org/10.1007/s10118-020-2390-1

[3] Porcarelli L., Shaplov A. S., Salsamendi M., Nair J. R., Vygodskii Y. S., Mecerreyes D., Gerbaldi C.: Single-ion block copoly(ionic liquid)s as electrolytes for all-solid state lithium batteries. ACS Applied Materials and Interfaces, **8**, 10350–10359 (2016). https://doi.org/10.1021/acsami.6b01973

[4] Nie H., Self J. L., Kuenstler A. S., Haywark R. C., de Alaniz J. T.: Multiaddressable photochromic architectures: From molecules to materials. Advanced Optical Materials, **7**, 1900224 (2019). https://doi.org/10.1002/adom.201900224

[5] Mokhtar A., Morinaga R., Akaishi Y., Shimoyoshi M., Kim S., Kurihara S., Kida T., Fukaminato T.: Reversible luminescence photoswitching of colloidal $CsPbBr_3$ nanocrystals hybridized with a diarylethene photoswitch. ACS Materials Letters, **2**, 727–735 (2020). https://doi.org/10.1021/acsmaterialslett.0c00131

[6] Lin Y-L., Tseng Y-H., Ho J-H., Chen Y-F., Chen J-T.: Photoswitchable composite polymer electrolytes using spiropyran-immobilized nanoporous templates. Chemistry: A European Journal, **27**, 14981–14988 (2021). https://doi.org/10.1002/chem.202102689

[7] Wang H., Zhu C. N., Zeng H., Ji X., Xie T., Yan X., Wu Z. L., Huang F.: Reversible ion-conducting switch in a novel single-ion supramolecular hydrogel enabled by photoresponsive host–guest molecular recognition. Advanced Materials, **31**, 1807328 (2019). https://doi.org/10.1002/adma.201807328

[8] Garg S., Schwartz H., Kozlowska M., Kanj A. B., Müller K., Wenzel W., Ruschewitz U., Heinke L.: Conductance photoswitching of metal-organic frameworks with embedded spiropyran. Angewandte Chemie-International Edition, **58**, 1193–1197 (2019). https://doi.org/10.1002/anie.201811458

[9] Yang J., Wang H., Wang J., Zhang Y., Guo Z.: Highly efficient conductivity modulation of cinnamate-based light-responsive ionic liquids in aqueous solutions. Chemical Communications, **50**, 14979–14982 (2014). https://doi.org/10.1039/c4cc04274c

[10] Zhang S., Liu S., Zhang Q., Deng Y.: Solvent-dependent photoresponsive conductivity of azobenzene-appended ionic liquids. Chemical Communications, **47**, 6641–6643 (2011). https://doi.org/10.1039/c1cc11924a

[11] Sumitani R., Mochida T.: Metal-containing poly(ionic liquid) exhibiting photogeneration of coordination network: Reversible control of viscoelasticity and ionic conductivity. Macromolecules, **53**, 6968–6974 (2020). https://doi.org/10.1021/acs.macromol.0c01141

[12] Nie H., Schauser N. S., Dolinski N. D., Hu J., Hawker C. J., Segalman R. A., Read de Alaniz J.: Light-controllable ionic conductivity in a polymeric ionic liquid. Angewandte Chemie-International Edition, **59**, 5123–5128 (2020). https://doi.org/10.1002/anie.201912921

[13] Hughes T., Simon G. P., Saito K.: Chemistries and capabilities of photo-formable and photoreversible crosslinked polymer networks. Materials Horizons, **6**, 1762–1773 (2019). https://doi.org/10.1039/c9mh00217k

[14] Li S., Jiang K., Wang J., Zuo C., Jo Y. H., He D., Xie X., Xue Z.: Molecular brush with dense PEG side chains: Design of a well-defined polymer electrolyte for lithium-ion batteries. Macromolecules, **52**, 7234–7243 (2019). https://doi.org/10.1021/acs.macromol.9b01641

[15] Chadwick R. C., Kardelis V., Liogier S., Adronov A.: Synthesis of conjugated polymers containing DIBAC-derived triazole monomers. Macromolecules, **46**, 9593–9598 (2013). https://doi.org/10.1021/ma4021467

[16] Chen G., Zhang F., Zhou Z., Li J., Tang Y.: A flexible dual-ion battery based on PVDF-HFP-modified gel polymer electrolyte with excellent cycling performance and superior rate capability. Advanced Energy Materials, **8**, 1801219 (2018). https://doi.org/10.1002/aenm.201801219

[17] Mouraliraman D., Shaji N., Praveen S., Nanthagopal M., Ho C. W., Karthik M. V., Kim T., Lee C. W.: Thermally stable PVDF-HFP-based gel polymer electrolytes for high-performance lithium-ion batteries. Nanomaterials, **12**, 1056–1069 (2022). https://doi.org/10.3390/nano12071056

[18] Ye Q., Liang H., Wang S., Cui C., Zeng C., Zhai T., Li H.: Fabricating a PVDF skin for PEO-based SPE to stabilize the interface both at cathode and anode for Li-ion batteries. Journal of Energy Chemistry, **70**, 356–362 (2022). https://doi.org/10.1016/j.jechem.2022.02.037

[19] Rong Z., Sun Y., Zhao Q., Cheng F., Zhang W., Chen J.: UV-cured semi-Interpenetrating polymer networks of solid electrolytes for rechargeable lithium metal batteries. Chemical Engineering Journal, **437**, 135329 (2022). https://doi.org/10.1016/j.cej.2022.135329

[20] Li W., Lynch V., Thompson H., Fox M. A.: Self-assembled monolayers of 7-(10-thiodecoxy)coumarin on gold: Synthesis, characterization, and photodimerization. Journal of the American Chemical Society, **119**, 7211–7217 (1997). https://doi.org/10.1021/ja970633m

[21] Kehrlösser D., Träger J., Kim H-C., Hampp N.: Synthesis and photochemistry of coumarin-based self-assembled monolayers on silicon oxide surfaces. Langmuir, **26**, 3878–3882 (2010). https://doi.org/10.1021/la903433r

[22] Ling J., Rong M. Z., Zhang M. Q.: Photo-stimulated self-healing polyurethane containing dihydroxyl coumarin derivatives. Polymer, **53**, 2691–2698 (2012). https://doi.org/10.1016/j.polymer.2012.04.016

[23] Chen Y., Jean C-S.: Polyethers containing coumarin dimer components in the main chain. I. Synthesis by photopolymerization of 7,7′-(polymethylenedioxy) dicoumarins. Journal of Applied Polymer Science, **63**, 1749–1758 (1997). https://doi.org/10.1002/(SICI)1097-4628(19970531)64:9<1749::AID-APP11>3.0.CO;2-T

[24] Chen Y., Jean C-S.: Polyethers containing coumarin dimer components in the main chain. II. Reversible photocleavage and photopolymerization. Journal of Applied Polymer Science, **64**, 1759–1768 (1997). https://doi.org/10.1002/(SICI)1097-4628(19970531)64:9<1759::AID-APP12>3.0.CO;2-T

[25] Zhu C. N., Li C. Y., Wang H., Hong W., Huang F., Zheng Q., Wu Z. L.: Reconstructable gradient structures and reprogrammable 3D deformations of hydrogels with coumarin units as the photolabile crosslinks. Advanced Materials, **33**, 2008057 (2021). https://doi.org/10.1002/adma.202008057

[26] Yonezawa N., Yoshida T., Hasegawa M.: Symmetric and asymmetric photocleavage of the cyclobutane rings in head-to-head coumarin dimers and their lactone-opened derivatives. Journal of the Chemical Society, Perkin Transactions, **1**, 1083–1086 (1983). https://doi.org/10.1039/P19830001083

[27] Du Z., Yan X., Dong R., Ke K., Ren B., Tong Z.: Unusual transient network and rheology of a photoresponsive telechelic associative model polymer in aqueous solution induced by dimerization of coumarin end groups. Macromolecules, **51**, 1518–1528 (2018). https://doi.org/10.1021/acs.macromol.7b01514

[28] Xu K.: Nonaqueous liquid electrolytes for lithium-based rechargeable batteries. Chemical Reviews, **104**, 4303–4418 (2004). https://doi.org/10.1021/cr030203g

[29] Armand M., Tarascon J-M.: Building better batteries. Nature, **451**, 652–657 (2008). https://doi.org/10.1038/451652a

[30] Baskoro F., Wong H. Q., Yen H-J.: Strategic structural design of a gel polymer electrolyte toward a high efficiency lithium-ion battery. ACS Applied Energy Materials, **2**, 3937–3971 (2019). https://doi.org/10.1021/acsaem.9b00295

[31] Long L., Wang S., Xiao M., Meng Y.: Polymer electrolytes for lithium polymer batteries. Journal of Materials Chemistry A, **4**, 10038–10069 (2016). https://doi.org/10.1039/c6ta02621d

[32] Chen P., Liu X., Wang S., Zeng Q., Wang Z., Li Z., Zhang L.: Confining hyperbranched star poly(ethylene oxide)-based polymer into a 3D interpenetrating network for a high-performance all-solid-state polymer electrolyte. ACS Applied Materials and Interfaces, **11**, 43146–43155 (2019). https://doi.org/10.1021/acsami.9b14346

[33] Narayan R., Chattopadhyay D. K., Sreedhar B., Raju K. V. S. N.: Cure, viscoelastic and mechanical properties of hydroxylated polyester melamine high solids coatings. Journal of Materials Science, **37**, 4911–4918 (2002). https://doi.org/10.1023/A:1020834818562